JACC Vol. 32, No. 1
July 1998:187–96

Characteristics of Wave Fronts During Ventricular Fibrillation in Human Hearts With Dilated Cardiomyopathy: Role of Increased Fibrosis in the Generation of Reentry

TSU-JUEY WU, MD,* JAMES J. C. ONG, MD, FACC, CHUN HWANG, MD, FACC, JOHN J. LEE, MD, FACC, MICHAEL C. FISHBEIN, MD, FACC, LAWRENCE CZER, MD, FACC, ALFREDO TRENTO, MD, CARLOS BLANCHE, MD, FACC, ROBERT M. KASS, MD, FACC, WILLIAM J. MANDEL, MD, FACC, HRAYR S. KARAGUEUZIAN, PHD, FACC, PENG-SHENG CHEN, MD, FACC

Los Angeles, California

Objectives. **We sought to evaluate the characteristics of wave fronts during ventricular fibrillation (VF) in human hearts with dilated cardiomyopathy (DCM) and to determine the role of increased fibrosis in the generation of reentry during VF.**

Background. **The role of increased fibrosis in reentry formation during human VF is unclear.**

Methods. **Five hearts from transplant recipients with DCM were supported by Langendorff perfusion and were mapped during VF. A plaque electrode array with 477 bipolar electrodes (1.6-mm resolution) was used for epicardial mapping. In heart no. 5, we also used 440 transmural bipolar recordings. Each mapped area was analyzed histologically.**

Results. **Fifteen runs of VF (8 s/run) recorded from the epicardium were analyzed, and 55 episodes of reentry were observed. The life span of reentry was short (one to four cycles), and the mean cycle length was 172 ± 24 ms. In heart no. 5, transmural scroll waves were demonstrated. The most common mode of initiation of reentry was epicardial breakthrough, followed by a line of conduction block parallel to the epicardial fiber orientation (34 [62%] of 55 episodes). In the areas with lines of block, histologic examination showed significant fibrosis separating the epicardial muscle fibers and bundles along the longitudinal axis of fiber orientation. The mean percent fibrous tissue in these areas (n = 20) was significantly higher than that in the areas without block (n = 28) (24 ± 7.5% vs. 10 ± 3.8%, p < 0.0001).**

Conclusions. **In human hearts with DCM, epicardial reentrant wave fronts and transmural scroll waves were present during VF. Increased fibrosis provides a site for conduction block, leading to the continuous generation of reentry.**

(J Am Coll Cardiol 1998;32:187–96)

Patients with dilated cardiomyopathy (DCM) have a high incidence of ventricular fibrillation (VF) and sudden cardiac death (1). Although the mechanisms are not completely understood, it is reasonable to hypothesize that morphologic changes of the heart from the disease process may contribute to the development of VF (1). Compatible with this hypothesis, previous histopathologic studies revealed significant interstitial, replacement and perivascular fibrosis in human ventricles with DCM (2–4). These fibrous tissues may enhance the nonuniform anisotropy and decrease the safety factor of impulse propagation (5,6), leading to conduction block and the development of reentry. The associations between conduction abnormalities or fibrosis and ventricular arrhythmias or sudden death have been described in various animal models of cardiomyopathies (7,8). Furthermore, increased fibrosis was also the cause for nonuniform anisotropic propagation (9) and fractionated electrograms (10) in patients with DCM. The severity of abnormal propagation correlated with the amount of increased fibrosis (9).

Previous mapping studies on the mechanisms of VF were performed primarily in normal animal ventricles (11,12). The activation patterns of VF in diseased human hearts, however, remain unknown. In this study, we obtained the hearts from transplant recipients. The explanted hearts were supported by

From the Division of Cardiology, Department of Medicine and Department of Pathology, Burns and Allen Research Institute, Cedars-Sinai Medical Center and University of California Los Angeles School of Medicine, Los Angeles, California. This study was performed during the tenure of an American College of Cardiology/Merck Research Fellowship (Drs. Ong and Hwang), a National Institutes of Health Individual Research Service Award (Dr. Ong), a National Institutes of Health Clinical Scientist Development Award (Dr. Ong), an ECHO Foundation Award (Dr. Karagueuzian) and an American Heart Association/Wyeth-Ayerst Established Investigatorship Award (Dr. Chen). The study was also supported in part by Specialized Center of Research (SCOR) Grant in Sudden Death P50HL52319 and FIRST Award R29HL50259 from the National Institutes of Health, Bethesda, Maryland and by the Ralph M. Parsons Foundation, Los Angeles, California.

Manuscript received September 12, 1997; revised manuscript received March 4, 1998, accepted March 17, 1998.

*Present address: Veterans General Hospital, Taichung, Taiwan.

Address for correspondence: Dr. Peng-Sheng Chen, Division of Cardiology, Room 5342, Cedars-Sinai Medical Center, 8700 Beverly Boulevard, Los Angeles, California 90048. E-mail: chenp@csmc.edu.

0735-1097/98/$19.00
PII S0735-1097(98)00184-3

Abbreviations and Acronyms
DCM = dilated cardiomyopathy
VF = ventricular fibrillation

Langendorff perfusion techniques (13,14) and were mapped with a computerized mapping system (11). Myocardial tissue in the mapped region was also analyzed histopathologically. The purposes of this study were 1) to evaluate the characteristics of wave fronts during VF in human hearts with DCM; and 2) to determine the role, if any, of increased fibrosis in the generation of reentry during VF.

Methods

Study group. This study included five consecutive patients with the clinical diagnosis of DCM and severe congestive heart failure who underwent orthotopic heart transplantation at Cedars-Sinai Medical Center from June to September 1995. The study protocol was approved by the Institutional Review Board. Table 1 summarizes the patient characteristics. All patients had normal coronary arteries on the coronary cineangiogram.

Langendorff preparation. After the heart of the transplant recipient was excised, the coronary arteries were perfused with cold, normal saline to decrease the myocardial temperature and to remove circulating antibodies and antigens. The heart was then immersed in cold, oxygenated Tyrode's solution and transported to the research laboratory immediately. The left and right coronary arteries were cannulated and perfused individually. The perfusate included 250 to 300 ml of washed, packed red blood cells from humans, swines or canines. The packed red blood cells were then mixed with 2000 ml of Tyrode's solution for the Langendorff perfusion. The Tyrode's solution had the following ionic composition in mmol/liter: NaCl 125, KCl 4.5, NaH_2PO_4 1.8, $CaCl_2$ 2.7, $MgCl_2$ 0.5, $NaHCO_3$ 24 and dextrose 5.5, in distilled deionized water (15).

To keep adequate coronary perfusion, the starting flow rate was 0.8 to 0.9 ml/g heart weight per minute (16). It was then adjusted to maintain a perfusion pressure of 50 to 70 mm Hg (16). The temperature was maintained at 37°C. Blood pH, partial pressure of oxygen, partial pressure of carbon dioxide and bicarbonate concentrations were monitored. Any abnormal value was promptly corrected. A blood sample was drawn at the end of the experiment to determine the hemoglobin level and serum electrolyte concentration.

Table 1. Clinical Characteristics of Heart Transplant Recipients

Pt. No./ Gender	Age (yr)	Diagnosis	LVEF (%)	Arrhythmia	Medication
1/F	40	DCM	0.16	Frequent PVCs	C, FU, I
2/M	44	DCM	0.15	Atrial flutter	D, E, FU
3/M	15	DCM	0.23	Atrial tachycardia, NSVT	D, C, FU
4/M	21	DCM	0.20	Frequent PVCs	C, FU
5/M	68	DCM	0.20	Chronic atrial fibrillation	D, E, FU, I

C = captopril; D = digoxin; DCM = dilated cardiomyopathy; E = enalapril; F = female; FU = furosemide; I = isordil; LVEF = left ventricular ejection fraction; M = male; NSVT = nonsustained ventricular tachycardia; PVCs = premature ventricular contractions.

Recording electrodes. The recording plaque electrode array for epicardial mapping was the same as that reported in Figure 1A of a previous report (11). The electrode array had 509 bipolar electrodes in 21 columns and 25 rows and measured 32 × 38 mm. The interelectrode distance was 1.6 mm. However, because of technical difficulties, data were acquired only with the last 477 electrodes.

Using previously published techniques for transmural mapping (17,18), 110 plunge electrodes were held within an acetal plate (Delrin, Du Pont) to form 11 columns and 10 rows with 5 mm between adjacent plunges. Each plunge electrode was constructed from a 21-gauge needle with eight recording terminals to make four bipolar recordings. The interelectrode distance was 3 mm. These 110 electrodes were plunged into the ventricular wall to obtain 440 simultaneous transmural recordings. As described previously (18), cell necrosis might occur but was confined to those myocytes immediately adjacent to the holes left by the plunge electrodes.

For both epicardial and transmural mappings, the electrodes were connected to a computerized mapping system (EMAP, Uniservices, Auckland, New Zealand) (11,19). The electrograms were filtered with a high pass filter of 0.5 Hz and a low pass filter of ~3 MHz and were acquired at 1,000 samples per second with a 16-bit accuracy.

Study protocol. All explanted hearts were attached to the Langendorff perfusion apparatus within 20 min after removal from the operative field. VF always occurred spontaneously during reperfusion and persisted for >1 h. We recorded at least three runs of VF (8 s/run) from the epicardium in each of the five hearts. Transmural mapping was also done in heart no. 5. At the completion of data acquisition, electrical shocks (10 to 30 J) were delivered through epicardial patch electrodes to terminate VF. The heart was then paced with twice the diastolic threshold current through bipolar electrodes from the edge (n = 5) and from the center (n = 4) of the recording electrode array. Patterns of epicardial activation were mapped while the ventricles were paced at cycle lengths of 500 to 600 ms. In heart nos. 4 and 5, VF was again induced by electrical stimulation.

Data analysis. The method for selecting the time of activation has been reported in detail previously (11,19). The patterns of activation were then displayed dynamically on the computer screen for visualization of the wave front during VF (11). To illustrate the regular pacing and transmural mapping data, conventional isochronal activation maps were constructed (18).

Histopathologic examination. At the conclusion of the experiments, the electrode array was removed. The coronary arteries were first perfused with 10% buffered formalin solu-

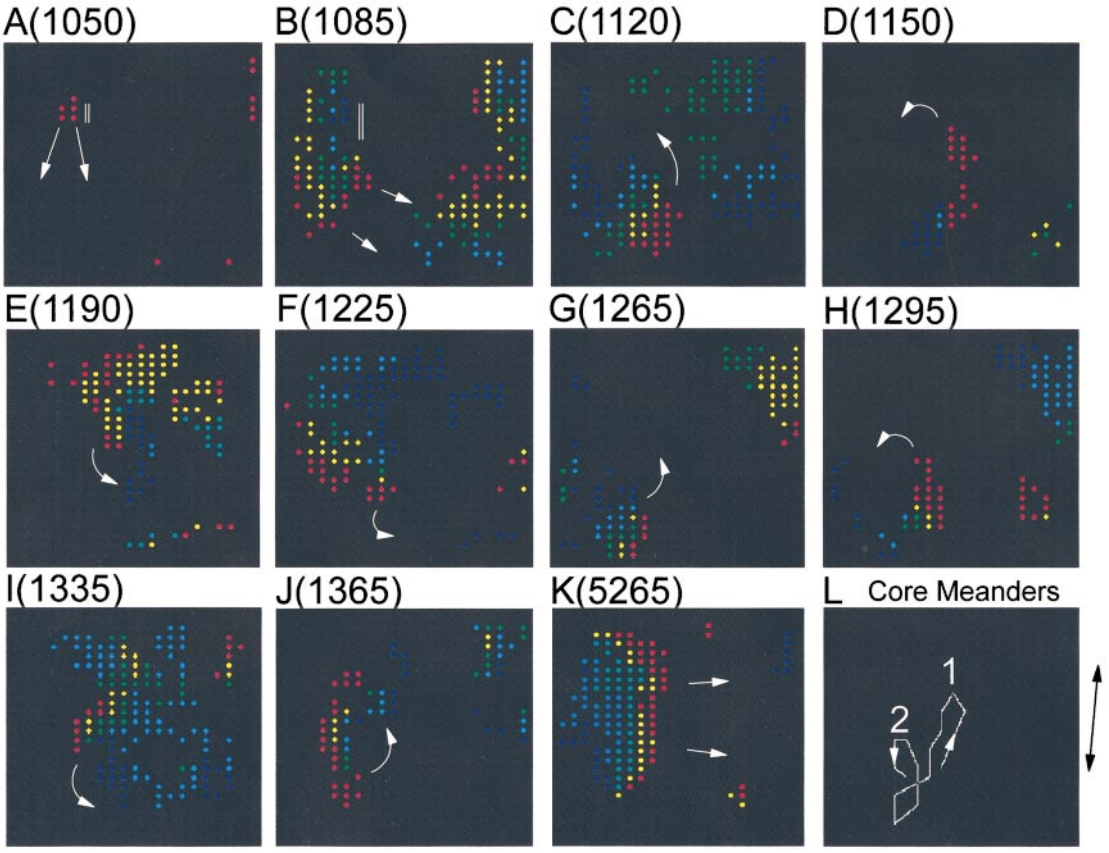

tion. The mapped tissue was then excised from the rest of the heart and fixed in the same solution for at least 48 h. Sections parallel to the epicardial surface (1 and 5 mm deep, respectively) were taken to determine the fiber orientation and the presence, if any, of an anatomic barrier. All tissue samples were processed routinely and were equally divided into four rectangular blocks. The edges of the blocks were marked with different colored inks to maintain orientation and then embedded in paraffin. Sections 5 μm thick were cut and stained with hematoxylin-eosin for light microscopic evaluation. To better demonstrate fibrous tissues separating the muscle fibers and bundles, trichrome staining was performed in selected specimens. We also used the point counting technique (3,4) to quantify the amount of fibrous tissue in the areas with and without abnormal impulse propagation. The area of tissue analyzed ranged from 10 to 15 mm^2 and >2,000 points were evaluated for each area. The number of cross points lying on fibrous tissue was divided by the total number of cross points evaluated to determine the percent fibrosis in each area.

Statistical analysis. All statistical analyses were performed using GB-Stat (20). Results are expressed as the mean value ± SD. Two-factor analysis of variance was used to determine if either of the following two factors was associated with the increased fibrosis: 1) the hearts studied; and 2) whether there was conduction block. A p value ≤0.05 was considered significant.

Figure 1. The reentrant wave fronts initiated by epicardial breakthrough with a line of conduction block parallel to the epicardial fiber orientation (data from heart no. 1). **Panels A to K** are selected frames from the dynamic display of the activation patterns during VF. **Panel L** shows the trajectory of the tip of the reentrant wave fronts, demonstrating the meandering nature of the core. Numbers 1 and 2 indicate the first and second cycles of reentry. The time of each frame is shown in parentheses above the panels. The beginning of the data acquisition was taken as time zero. The myocardial fiber orientation is displayed by the **double-headed arrow** at the right lower border of the figure.

Results

The five explanted hearts weighed 494 ± 46 g (range 430 to 550). VF was mapped from the epicardium of the left (heart nos. 1 and 5) or the right (heart nos. 2, 3 and 4) ventricle. Transmural mapping was performed in the right ventricle of heart no. 5. At the end of the experiments, the potassium concentrations ranged from 3.5 to 4.3 mmol/liter, and the hemoglobin levels ranged from 2.7 to 4.4 g/dl.

Reentrant wave fronts in VF. Fifteen runs of VF recorded from the epicardium (three runs from each heart) were analyzed, with a total duration of 120 s. In these 15 runs of VF, 55 episodes of reentrant wave fronts (3.7 ± 1.5 episodes for each run of VF [range 2 to 7]) were observed in the mapped region. The mean number of rotations (life span) was 1.5 ± 0.7

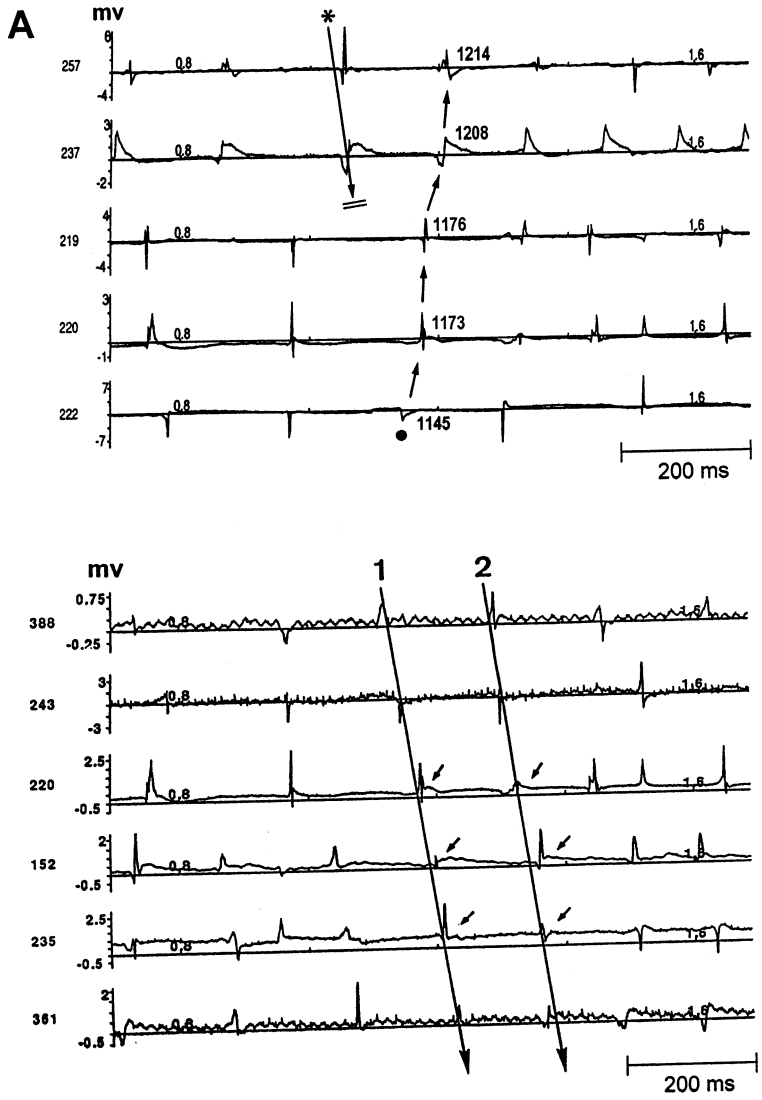

Figure 2. The actual activations registered in Figure 1. The numbers on the left edge of each panel indicate the electrode numbers and the location in the electrode array. Numbers 0.8 and 1.6 indicate the times in seconds, with the onset of data acquisition as time zero. In **panel A,** the activations of epicardial breakthrough **(long arrow with asterisk)** failed to travel across the site between channels 237 and 219, leading to conduction block and the initiation of reentry. The activations with corresponding activation times (ms) from channels 222 to 257 **(solid circle followed by short arrows)** illustrate part of the first cycle of the reentrant loop. Note that conduction delay (1208 − 1176 = 32 ms) was present when the wave front propagated through the site between channels 219 and 237. In **panel B,** these activations show that the reentrant excitations **(long arrows)** persisted for two rotations. Numbers 1 and 2 indicate the first and second reentrant cycles.

(range 1 to 4), and the mean cycle length was 172 ± 24 ms (range 135 to 240 s). In 25 episodes the reentry was clockwise, and in 30 episodes it was counterclockwise.

Initiation of reentry. During VF, two patterns of initiation of new reentrant wave fronts were observed. In 34 (62%) of 55 episodes, the reentrant wave fronts were initiated by epicardial breakthrough with a line of conduction block parallel to the epicardial fiber orientation. In 16 (29%) of 55 episodes, reentry was initiated by a wave front crossing roughly perpendicular to the tail of another wave front, creating a wave break (11). In 5 (9%) of 55 episodes, the mechanism of reentry initiation could not be determined because the wave fronts entered the mapped region from the edge of mapped tissue after they were already initiated.

Figure 1 shows an example of reentrant wave front initiated by epicardial breakthrough. In panel A, a wave front first occurred in the left upper part of the mapped region. Panel B shows that the wave front spread downward to the periphery, with conduction block at one side of the wave front (double line). This line of block was roughly parallel to the epicardial fiber orientation. Panels B through D show that the wave front distal to the line of block propagated slowly across the epicardial fiber orientation and initiated two complete cycles of counterclockwise reentry (panels C to J). Panel K shows that a large wave front propagated through the area of conduction block shown in panel B. Panel L shows the path and direction (arrows) of the leading inner point (tip) of the reentrant wave front for two cycles (11). Meandering of the core toward the left lower edge of the mapped region was apparent. Figure 2 shows the actual activations registered in Figure 1. In panel A, the upper two channels (channels 257 and 237) registered the activations of epicardial breakthrough in panel B of Figure 1 (long arrow with asterisk). The wave front failed to travel across the site between channels 237 and 219, leading to conduction block and the initiation of reentry. The subsequent activations from channel 222 to 257 (filled circle followed by short arrows) illustrate part of the first cycle of the reentrant loop. Note that conduction delay was present when the wave

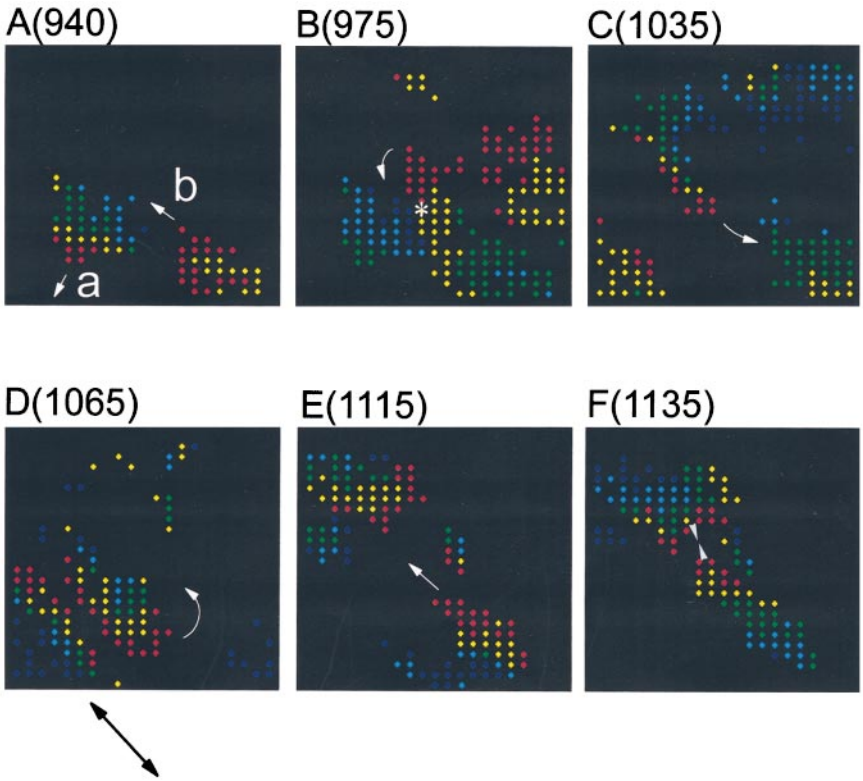

Figure 3. The reentrant wave front initiated by perpendicular intersection of two wave fronts (data from heart no. 5). **Panel A** shows that waves "a" and "b" interact at a right angle. The asterisk in **panel B** indicates the point of wave break. The wave break was then followed by one rotation of counterclockwise reentry (**panels B to F).** The reentry was terminated owing to collision of wave fronts **(arrows in panel F).** The myocardial fiber orientation is displayed by the **double-headed arrow** at the left lower border of the figure.

front propagated through the site between channels 219 and 237. Panel B shows that reentrant excitations (long arrows) persisted for two rotations. There are obvious differences in the amplitude and the direction of local electrograms in the same channel between the first and second cycles (short arrows). These changes could be explained by the meandering nature of the core (11,21,22).

To determine the conduction characteristics around the line of block shown in panel B of Figure 1, two runs of VF (16 s in duration) recorded from the same mapped region were evaluated. During this period, 96 wave fronts encountered the site of block. Among them, 20 wave fronts (21%), usually large ones, propagated across this site. In the remaining 76 wave fronts (79%), conduction block occurred at the same site. After the block, 48 wave fronts terminated, 22 wave fronts circled around the site of block but did not result in a reentrant circuit and 6 wave fronts initiated complete reentry. These findings indicate that the conduction block was not absolute at this site. Large and coherent wave fronts may propagate across the same area without block, as shown in Figure 1K.

Figure 3 demonstrates an example of initiation of reentry by wave break. Panel A shows a wave front (wave "a") that first appeared at the center of the mapped region and propagated toward the left lower corner. A second wave front (wave "b") propagated from the right lower corner toward the center of mapped region. The perpendicular intersection of these two wave fronts resulted in a wave break (panel B, asterisk) and initiated one cycle of reentry (panels B to F). The reentry was terminated due to collision of wave fronts (panel F). Figure 4 shows the actual activations registered in Figure 3. The lower three channels (channels 345, 364 and 384) registered wave "a" in Figure 3A, and the upper three channels (channels 454, 432 and 368) registered wave "b" in the same panel. The local activations recorded at channel 304 show that wave "b" entered the same area 75 ms (i.e., intersection interval) (11) after wave "a" activated this area. Figure 4 also shows parts of the reentrant loop (arrows with asterisk) after perpendicular intersection. As demonstrated previously (11), the intersection intervals of the 16 episodes, which show initiation of reentry by a wave break in this study, did not distribute randomly. Rather, these intervals clustered between 65 and 96 ms (mean 80 ± 10).

Termination of reentry. Thirty-eight (69%) of 55 episodes of reentrant wave fronts terminated because of interference with other wave fronts (11). In 10 episodes (18%), they terminated spontaneously (11,23). In the remaining 7 episodes (13%), the mode of termination could not be determined because the reentrant wave fronts meandered outside the mapped region.

Nonreentrant wave fronts in VF. The majority of wave fronts mapped on the epicardium did not participate in the formation of reentry. A significant number of nonreentrant wave fronts had the earliest activation site within the mapped region, resulting from epicardial breakthrough (11). The incidence of epicardial breakthrough within the mapped region was 42 ± 11 times per run of VF.

A significant number of these wave fronts (6.5 ± 1.4 times per run of VF) initiated incomplete rotating circuits (Fig. 5). In such cases, the wave fronts rotated around a line of conduction

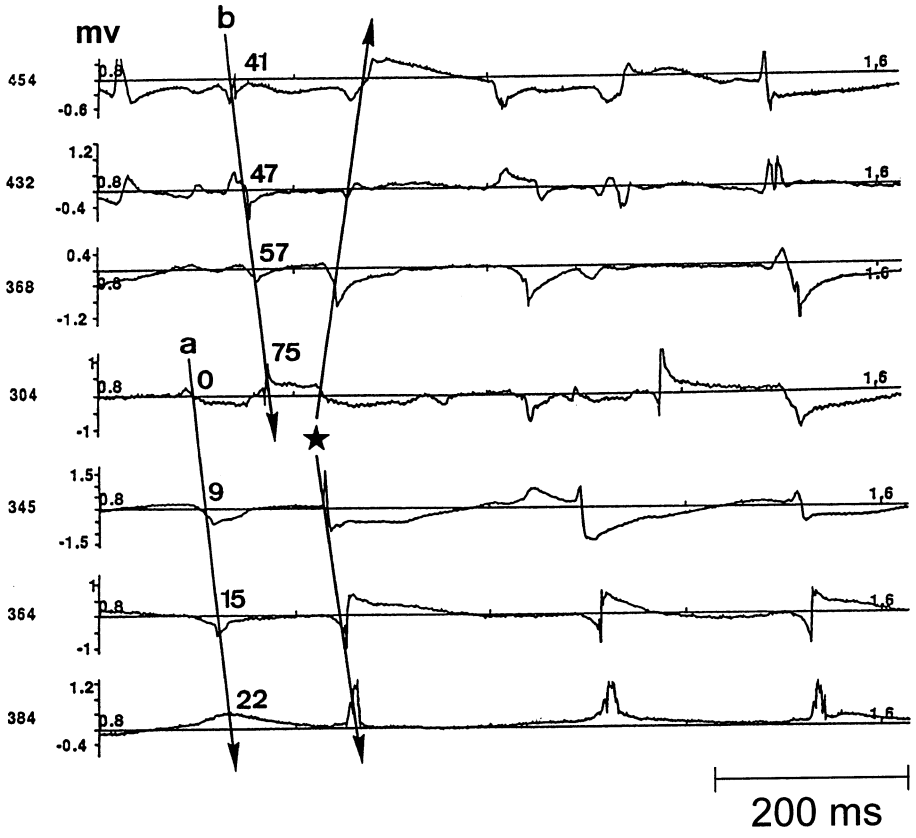

Figure 4. The actual activations registered in Figure 3. Wave "b" collided with the tail of wave "a" at or near channel 304, and initiated reentry. The activations recorded at channel 304 show that wave "b" propagated to this area 75 ms (i.e., intersection interval) after it was activated by wave "a". The **arrows with an asterisk** indicate parts of a reentrant loop.

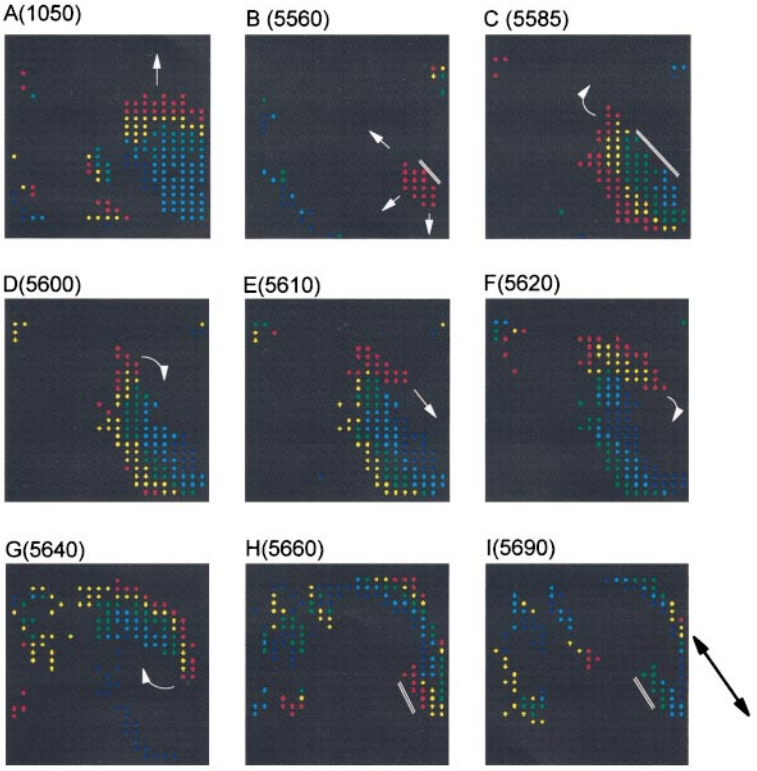

Figure 5. An example of incomplete rotating circuit (data from heart no. 5). **Panel A** shows a wave front propagating through the area of conduction block, which is shown in **panels B and C.** After conduction block occurred, a rotating wave front was initiated **(panels D to G)** but had spontaneous termination **(panels H and I).** At the time of termination, the line of block was parallel to the fiber orientation. The myocardial fiber orientation is displayed by the **double-headed arrow** at the right lower border of the figure.

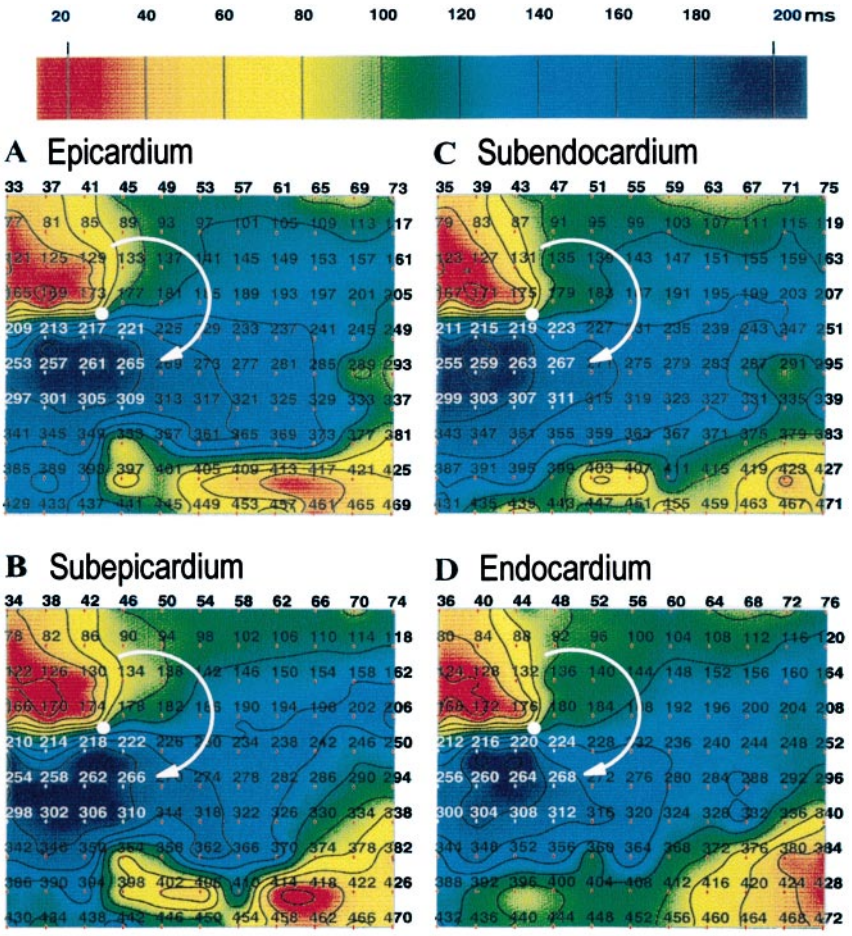

Figure 6. Isochronal maps demonstrating transmural scroll waves during VF from the right ventricle of heart no. 5. Times of activation are colored-coded according to the color bar above the panels. The numbers in the electrode arrays indicate the location and the numbers of the bipolar recording electrodes. From epicardium, subepicardium, subendocardium to endocardium **(panels A to D),** there were only small differences in the transmural distribution of activation patterns. The filament of this scroll wave (**line connecting white circles** near channels 217, 218, 219 and 220) was perpendicular to the surface of the ventricular wall. The **white arrow** in each panel indicates the rotating direction of the scroll wave.

block parallel to the epicardial fiber orientation (Fig. 5, B and C), which was similar to that shown in Figure 1. However, the rotating wave front was either terminated by interference or had spontaneous termination (Fig. 5, H and I).

Transmural plunge electrode mapping. Transmural mapping in one heart documented the presence of reentrant wave fronts during VF in three dimensions (scroll waves). As was observed in canine VF (18), the reentrant wave fronts (three episodes with life spans of 1, 2 and 2 cycles, respectively) recorded from the right ventricle of heart no. 5 show only small differences in the transmural distribution of activation patterns (Fig. 6). The resultant straight vortex filament was perpendicular to the surface of the ventricular wall.

Activation patterns during regular pacing. During regular pacing from the edge and from the center of the recording electrode array at cycle lengths of 500 to 600 ms, the epicardial isochronal maps showed no evidence of conduction block in any of the hearts studied. When the paced wave fronts propagated across the epicardial fiber orientation, slow conduction (<0.20 m/s) was consistently observed over the areas that served as sites of conduction block during VF. In contrast, the mean conduction velocity along the epicardial fiber orientation was 0.66 ± 0.09 m/s (range 0.54 to 0.78) (n = 5). This would represent an anisotropic conduction velocity ratio >2.5:1. However, because transverse conduction velocity varies greatly depending on the underlying histologic changes, it was difficult to estimate the accurate anisotropic conduction velocity ratio in these hearts. These results were compatible with the findings reported by Anderson et al. (9).

Histopathologic findings. From each explanted heart, myocardial fiber orientation could be clearly shown in sections of the mapped region. Significant fibrosis was the consistent finding in all hearts at two different levels of sections. However, these fibrous tissues were distributed unevenly. An increase of fibrous tissues separating the epicardial muscle fibers and bundles along the longitudinal axis of fiber orientation was demonstrated by trichrome staining (Fig. 7 and 8). In Figure 7, significant interstitial, replacement and perivascular fibrosis in panels C and E corresponded to the area of conduction block in Figure 1. In the areas without conduction block, however, histologic examination showed either normal tissue (panel A) or mild fibrosis (panel D). Similarly, in Figure 8, increased fibrosis (panel C) corresponded to the line of conduction block in Figure 5. The amount of fibrous tissue in panel C was higher than that in the areas without conduction block (panels A and D). In each heart, the percent fibrous tissue was quantified in three to five areas with lines of conduction block and in five to six areas not serving as sites of conduction block. Two-factor

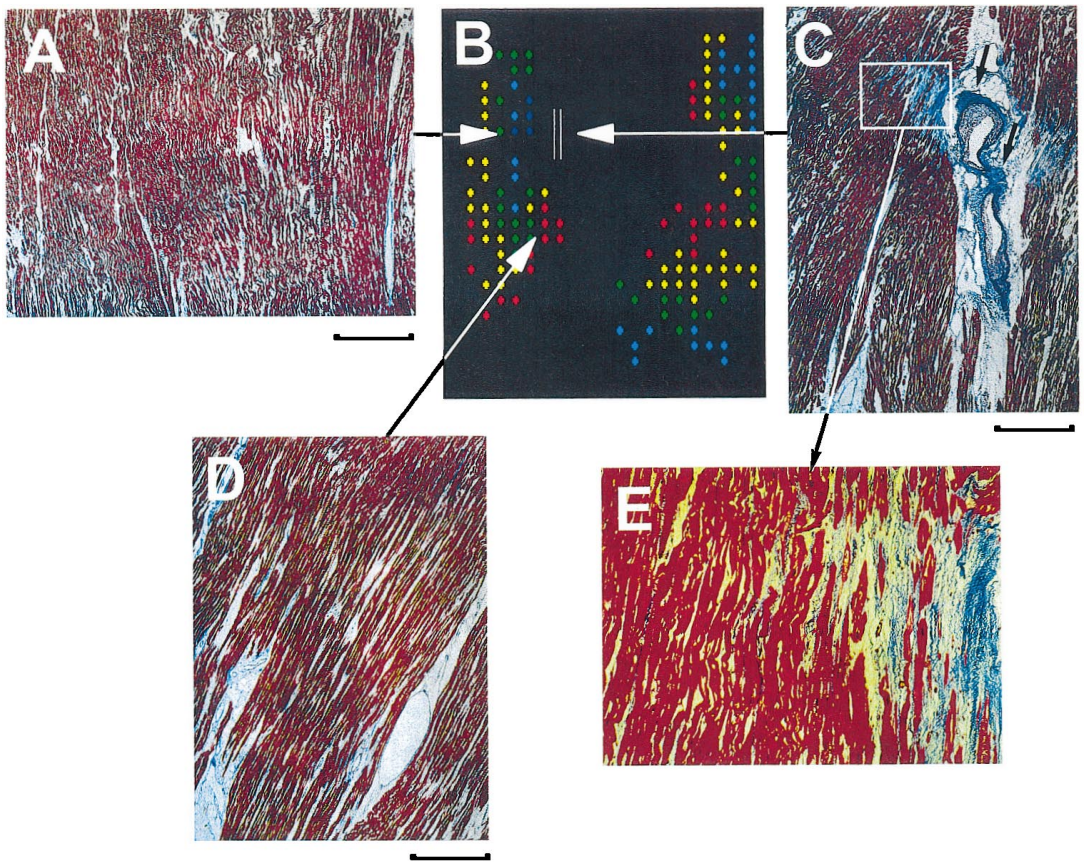

Figure 7. Histologic findings corresponding to activations shown in Figure 1. **Panels A, C, D and E** show sections of the left ventricular myocardium parallel to the epicardium in heart no. 1. With trichrome stain, small veins with perivascular fibrosis **(blue areas)** were clearly seen in **panel C (arrows).** The magnified view **(panel E)** also showed interstitial and replacement fibrosis. The areas of fibrosis in **panels C and E** corresponded to the line of conduction block in **panel B** (same frame as Fig. 1B). However, in the areas without conduction block, histologic examination showed either normal tissue **(panel A)** or mild fibrosis **(panel D).** Original magnification 10×, panels A, C and D; 100×, panel E. Calibration lines 1 mm.

analysis of variance showed that the mean percent fibrous tissue was not different among the five hearts studied ($p = 0.48$). However, the mean percent fibrous tissue in the areas with lines of conduction block ($n = 20$) was significantly higher than that in the areas not serving as sites of conduction block ($n = 28$) ($24 \pm 7.5\%$ vs. $10 \pm 3.8\%$, $p < 0.0001$).

Discussion

To our knowledge, this is the first study to use computerized mapping techniques to study human VF and to correlate the activation patterns of VF with the underlying pathologic findings in diseased human ventricles. We found that both wandering wavelets and short-lived epicardial reentrant wave fronts were present in human VF. In one heart, three episodes of transmural scroll waves were also registered. Although these organized reentrant wave fronts may serve as a source of activation, they are infrequently observed during VF both in normal canine ventricles (11) and in the diseased human ventricles of this study. Because of their scarcity, the relevance of these wave fronts to the perpetuation of VF remains unclear.

Increased fibrosis and initiation of reentrant wave fronts. In normal canine ventricles (11), the new reentrant wave fronts during VF were consistently initiated by an interaction between two propagating wave fronts roughly perpendicular to each other. In the cardiomyopathic human hearts, however, only ~30% of the new reentrant wave fronts were initiated by this mechanism. Most of the new reentrant wave fronts (62%) were initiated by epicardial breakthrough, followed by a line of conduction block parallel to the epicardial fiber orientation. These findings suggest the importance of increased fibrosis (i.e., increased tissue anisotropy) in the initiation of reentry.

Anisotropic conduction is believed to play an important role in the pathogenesis of various atrial and ventricular arrhythmias. Dillon et al. (24) showed that anisotropic conduction and block may result from muscle fiber separation in the epicardial border zone of subacute canine infarcts. Spach and Dolber (6) reported that the greater incidence of atrial arrhythmias with age may be caused by the development of extensive collagenous septa dividing the myocardial fibers. Apart from broad bands of scarring, interstitial fibrosis was another structural complexity characteristic of slow conduction

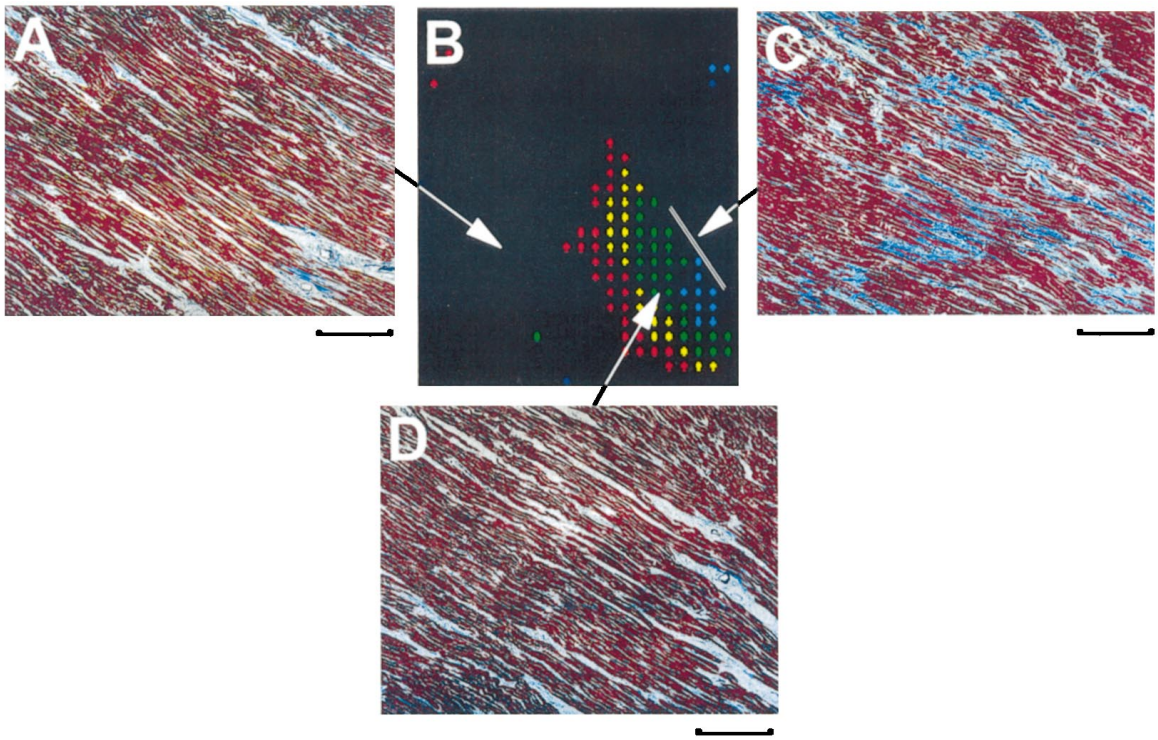

Figure 8. Histologic findings corresponding to activations shown in Figure 5. **Panels A, C and D** show sections of the subepicardial myocardium from the left ventricle of heart no. 5. With trichrome stain, significant interstitial fibrosis (**blue area**) was demonstrated in **panel C.** The area of fibrosis corresponded to the line of conduction block in **panel B** (same frame as Fig. 5C). In the areas without conduction block, however, histologic examination showed less fibrous tissue (**panels A and D).** Original magnification 10×, panels A, C and D. Calibration lines 1 mm.

and delayed activation in animals or patients with myocardial infarction (25,26). It is also known that there is an association between increased fibrosis and nonuniform anisotropic propagation in human hearts with DCM (9,10). Our results are compatible with these studies.

In this study, histologic examination showed significant fibrosis in each heart. An increase of fibrous tissues between muscle fibers and bundles may enhance nonuniform anisotropy and promote electrical uncoupling (5,6). Impulse propagation may fail in the transverse direction but not in the longitudinal propagation, resulting in unidirectional conduction block (27,28). Once a line of conduction block parallel to the fiber orientation occurs, the area distal to the line of block may become activated by the slowly propagating transverse wave front. This provides a longer delay for the proximal fibers to regain excitability and for reentry to occur (Fig. 1). The correlation between the lines of conduction block and increased fibrosis suggests the importance of tissue abnormalities in the initiation of new reentrant wave fronts. Although we do not have Langendorff-perfused normal human hearts for comparison, the incidence of reentrant wave fronts in our study was higher than that reported in normal canine ventricles (55 episodes in 120 s of human VF vs. 12 episodes in 180 s of canine VF using the same mapping electrode array) (11).

Anatomic versus functional reentry. Although increased fibrosis decreased the safety factor of impulse propagation across the myocardial fibers, the conduction block was not absolute. Large and coherent wave fronts during paced rhythm or during VF (Fig. 1K and 5A) were able to propagate across the areas with increased fibrosis. In contrast to larger wave fronts, smaller wavelets (Fig. 1A and 5B) often ceased propagation when they encountered these same areas. These findings indicate that successful conduction or block was determined not only by the underlying histologic changes but also by the source-sink ratio (29,30). Large and coherent wave fronts are better sources for impulse propagation than the small wavelets; therefore, larger wave fronts have a better chance to excite the cells downstream (sink). These findings also indicate that there may not be a clear distinction between functionally and anatomically based reentry in diseased human ventricles.

Excitable gap of reentrant wave fronts. In this study, the mean cycle length of reentrant wave fronts was 172 ± 24 ms. However, the mean intersection interval (11), which represents the refractory period of the VF wave front, was only 80 ± 10 ms. These findings suggest that a large, excitable gap may be present in the reentrant wave fronts during human VF. The presence of a large, excitable gap may explain the observation that the most common mode of termination of reentrant wave fronts was outside interference, and that the reentrant wave fronts had short life spans.

Study limitations. There are several limitations of the present study. First, these ventricles were Langendorff perfused and denervated. Whether reperfusion and denervation affect the patterns of activation in VF is unclear. Second, all five patients were taking a combination of different medications including digoxin. These drugs may alter the electrophysiologic properties of explanted hearts and may affect the characteristics of VF. Third, because only a small region of the ventricles can be mapped, the global patterns of activation during human VF remain unclear.

Conclusions. In human hearts with DCM supported by Langendorff perfusion, both organized epicardial reentrant wave fronts and transmural scroll waves were present during VF. The most common mode of initiation of new reentrant wave fronts during VF was related to the conduction block caused by altered tissue anatomy. Increased fibrosis provides a site for conduction block, leading to the continuous generation of reentry.

We thank Dustan Hough for developing the dynamic display program; Peter Hunter, PhD, David Bullivant, PhD, Sylvain Martel and Serge LaFontaine for constructing the mapping system; Avile McCullen, Meiling Yuan, Paul Nusser, RN and Deborah Harasty, RN, for technical assistance; and Elaine Lebowitz for secretarial assistance. We also acknowledge the advice and training provided by Michiel J. Janse, MD, Amsterdam, The Netherlands, in establishing Langendorff perfusion techniques in our laboratory.

References

1. Packer M. Sudden unexpected death in patients with congestive heart failure: a second frontier. Circulation 1985;72:681–5.
2. Anderson KR, Sutton MG, Lie JT. Histopathological types of cardiac fibrosis in myocardial disease. J Pathol 1979;128:79–85.
3. Schwarz F, Mall G, Zebe H, et al. Quantitative morphologic findings of the myocardium in idiopathic dilated cardiomyopathy. Am J Cardiol 1983;51: 501–6.
4. Unverferth DV, Baker PB, Swift SE, et al. Extent of myocardial fibrosis and cellular hypertrophy in dilated cardiomyopathy. Am J Cardiol 1986;57:816–20.
5. Spach MS, Miller WT Jr, Dolber PC, et al. The functional role of structural complexities in the propagation of depolarization in the atrium of the dog: cardiac conduction disturbances due to discontinuities of effective axial resistivity. Circ Res 1982;50:175–91.
6. Spach MS, Dolber PC. Relating extracellular potentials and their derivatives to anisotropic propagation at a microscopic level in human cardiac muscle: evidence for electrical uncoupling of side-to-side fiber connections with increasing age. Circ Res 1986;58:356–71.
7. Fein FS, Capasso JM, Aronson RS, et al. Combined renovascular hypertension and diabetes in rats: a new preparation of congestive cardiomyopathy. Circulation 1984;70:318–30.
8. Bakth S, Arena J, Lee W, et al. Arrhythmia susceptibility and myocardial composition in diabetes: influence of physical conditioning. J Clin Invest 1986;77:382–95.
9. Anderson KP, Walker R, Urie P, et al. Myocardial electrical propagation in patients with idiopathic dilated cardiomyopathy. J Clin Invest 1993;92:122–40.
10. de Bakker JMT, van Capelle FJL, Janse MJ, et al. Fractionated electrograms in dilated cardiomyopathy: origin and relation to abnormal conduction. J Am Coll Cardiol 1996;27:1071–8.
11. Lee JJ, Kamjoo K, Hough D, et al. Reentrant wave fronts in Wiggers' stage II ventricular fibrillation: characteristics, and mechanisms of termination and spontaneous regeneration. Circ Res 1996;78:660–75.
12. Kenknight BH, Bayly PV, Gerstle RJ, et al. Regional capture of fibrillating ventricular myocardium: evidence of an excitable gap. Circ Res 1995;77:849–55.
13. Langendorff O. Über elektrische Reizung des Herzens. Arch Anat Physiol 1885:284.
14. Durrer D, van Dam RTh, Freud GE, et al. Total excitation of the isolated human heart. Circulation 1970;41:899–912.
15. Ikeda T, Uchida T, Hough D, et al. Mechanism of spontaneous termination of functional reentry in isolated canine right atrium: evidence for the presence of an excitable but nonexcited core. Circulation 1996;94:1962–73.
16. Döring HJ, Dehnert H. The Isolated Perfused Warm-Blooded Heart According to Langendorff. Ithaca (NY): Transonic Systems, Inc., 1988:1–130.
17. Chen P-S, Shibata N, Wolf P, et al. Activation during ventricular defibrillation in open-chest dogs: evidence of complete cessation and regeneration of ventricular fibrillation after unsuccessful shocks. J Clin Invest 1986;77:810–23.
18. Chen P-S, Wolf P, Dixon EG, et al. Mechanism of ventricular vulnerability to single premature stimuli in open chest dogs. Circ Res 1988;62:1191–209.
19. Bonometti C, Hwang C, Hough D, et al. Interaction between strong electrical stimulation and reentrant wavefronts in canine ventricular fibrillation. Circ Res 1995;77:407–16.
20. Friedman P. GB-Stat. Silver Spring (MD): Dynamic Microsystems, Inc., 1995.
21. Gray RA, Jalife J, Panfilov AV, et al. Mechanisms of cardiac fibrillation. Science 1995;270:1222–3.
22. Starmer CF, Romashko DN, Reddy RS, et al. Proarrhythmic response to potassium channel blockade: numerical studies of polymorphic tachyarrhythmias. Circulation 1995;92:595–605.
23. Cha YM, Birgersdotter-Green U, Wolf PL, Peters BB, Chen P-S. The mechanism of termination of reentrant activity in ventricular fibrillation. Circ Res 1994;74:495–506.
24. Dillon SM, Allessie MA, Ursell PC, Wit AL. Influences of anisotropic tissue structure on reentrant circuits in the epicardial border zone of subacute canine infarcts. Circ Res 1988;63:182–206.
25. Ursell PC, Gardner PI, Albala A, Fenoglio JJ, Wit AL. Structural and electrophysiological changes in the epicardial border zone and canine myocardial infarcts during infarct healing. Circ Res 1985;56:436–51.
26. Pogwizd SM, Hoyt RH, Saffitz JE, et al. Reentrant and focal mechanisms underlying ventricular tachycardia in the human heart. Circulation 1992;86: 1872–87.
27. Delgado C, Steinhaus B, Delmar M, Chialvo DR, Jalife J. Directional differences in excitability and margin of safety for propagation in sheep ventricular epicardial muscle. Circ Res 1990;67:97–110.
28. Delmar M, Michaels DC, Johnson T, Jalife J. Effects of increasing intercellular resistance on transverse and longitudinal prolongation in sheep epicardial muscle. Circ Res 1987;60:780–5.
29. Cabo C, Pertsov AM, Baxter WT, et al. Wavefront curvature as a cause of slow conduction and block in isolated cardiac muscle. Circ Res 1994;75: 1014–28.
30. Ong JJC, Cha YM, Kriett JM, et al. The relation between atrial fibrillation wavefront characteristics and accessory pathway conduction. J Clin Invest 1995;96:2284–96.